Effect of different cosmologies on the galaxy stellar mass function

Amanda R. Lopes,[1,2]★† C. Gruppioni,[2] M. B. Ribeiro,[1,3] L. Pozzetti,[2] S. February,[4] O. Ilbert[5] and F. Pozzi[6]

[1]*Observatório do Valongo, Universidade Federal do Rio de Janeiro, RJ 20080-090, Brazil*
[2]*INAF – Osservatorio Astronomico di Bologna, Via Ranzani 1, I-40127 Bologna, Italy*
[3]*Instituto de Física, Universidade Federal do Rio de Janeiro, RJ 21941-972, Brazil*
[4]*Centre for High Performance Computing, CSIR, 15 Lower Hope St., Rosebank, Cape Town 7700, South Africa*
[5]*Aix Marseille Université, CNRS, LAM (Laboratoire d'Astrophysique de Marseille), UMR 7326, F-13388 Marseille, France*
[6]*Dipartimento di Astronomia, Università di Bologna, via Ranzani 1, I-40127 Bologna, Italy*

ABSTRACT

The goal of this paper is to understand how the underlying cosmological models may affect the analysis of the stellar masses in galaxies. We computed the galaxy stellar mass function (GSMF) assuming the observationally constrained Lemaître–Tolman–Bondi (LTB) 'giant-void' models and compared them with the results from the standard cosmological model. Based on a sample of 220 000 K_S-band selected galaxies from the UltraVISTA data, we computed the GSMF up to $z \approx 4$ assuming different cosmologies, since, from a cosmological perspective, the two quantities that affect the stellar mass estimation are the luminosity distance and time. The results show that the stellar mass decreased on average by $\sim$1.1–27.1 per cent depending on the redshift value. For the GSMF, we fitted a double-Schechter function to the data and verified that a change is only seen in two parameters, $\mathcal{M}^*$ and ϕ_1^*, but always with less than a 3σ significance. We also carried out an additional analysis for the blue and red populations in order to verify a possible change on the galaxy evolution scenario. The results showed that the GSMF derived with the red population sample is more affected by the change of cosmology than the blue one. We also found out that the LTB models overestimated the number density of galaxies with $\mathcal{M} < 10^{11}\,\mathcal{M}_\odot$, and underestimate it for $\mathcal{M} > 10^{11}\,\mathcal{M}_\odot$, as compared to the standard model over the whole studied redshift range. This feature is noted in the complete, red plus blue, sample. Once we compared the general behaviour of the GSMF derived from the alternative cosmological models with the one based on the standard cosmology we found out that the variation was not large enough to change the shape of the function. Hence, the GSMF was found to be robust under this change of cosmology. This means that all physical interpretations of the GSMF based in the standard cosmological model are valid on the LTB cosmology.

Key words: galaxies: evolution – galaxies: luminosity function, mass function – galaxies: stellar content – cosmology: theory.

1 INTRODUCTION

The estimation of the galactic stellar mass, i.e. mass contained in the form of stars, has become standard in the study of galaxy evolution. This is based on the broad-band spectral energy distribution (SED) fitting, which uses multiwavelength photometry observational data to calculate the galaxy physical properties through the application of a series of models and assumptions (see Walcher et al. 2011, for a review). This technique relies on the choice of a number of astrophysical parameters, such as the stellar population synthesis (SPS) models (e.g. Bruzual & Charlot 2003; Maraston 2005; for a review see Conroy 2013), a grid of metallicity, an extinction law, an initial mass function (IMF) and a cosmological model. The SED-fitting programmes (e.g. *Le Phare*, *MAGPHYS*, *HyperZ*) were written assuming the cold dark matter cosmological model with a cosmological constant (ΛCDM; e.g. Komatsu et al. 2009), which now is adopted as a standard cosmology. Hence, the whole analysis based on this procedure is dependent on the assumed cosmological model. But, how does the assumption of the underlying cosmology

★ E-mail: amanda05@astro.ufrj.br, amandalopes1920@gmail.com
† Present address: Observatório Nacional, Rua General José Cristino, Rio de Janeiro, Brazil.

influence the derivation of the main physical parameters? And how strong is this influence? These are some of the questions we aim to answer.

The cosmic time evolution of the stellar mass can be studied through the galaxy stellar mass function (GSMF), which describes the number density of galaxies per logarithmic stellar mass interval. This function is a well-established tool to understand how the mass in galaxies evolve and which physical processes are involved. Several works calculating and fitting the GSMF by a simple or double Schechter function in different redshift ranges can be found in the literature, e.g. McLure et al. (2009), Domínguez-Sánchez et al. (2011), Mortlock et al. (2011), Baldry et al. (2012), down to low-mass limits ($\mathcal{M} \sim 10^8 \mathcal{M}_\odot$). However, all the analyses with this function present a cosmological model dependence related to both the stellar mass and the comoving volume. And although one might argue that the current precision for the constraints on the cosmological model are good enough to render a similar GSMF in all cosmologies fitted by the observations, this assertion has, nevertheless, never been tested. So, the question remains on how robust is the GSMF under a change of cosmology.

Moreover, the future ESA mission Euclid (Joachimi 2016) aims at improving the cosmological probes, providing clues on the nature of dark matter and dark energy and testing Einstein's theory of gravity at larger scales. Hence, non-standard cosmology simulations, including galaxy properties, will be necessary. Even though, this work does not simulate the whole Universe, it will give us an estimate of how much the galaxies, or the galaxy stellar masses, change when a non-standard cosmology is assumed.

The main goal of this paper is to estimate the influence of different cosmologies on the galaxy physical parameters, particularly referring to the stellar mass and mass function derivation. However, the uncertainties on these quantities have been extensively discussed only in terms of IMF, SPS, etc. For example, Conroy, Gunn & White (2009) studied the stellar masses derivation using SED technique and found a variation of about 0.3 dex if the uncertainties related to all astrophysical assumptions were taken into account. Other papers emphasized the importance of a specific assumption in the stellar mass results, e.g. star formation history (SFH; Maraston et al. 2010; Pforr, Maraston & Tonini 2012), the SPS model (Wuyts et al. 2007; Cimatti et al. 2008; Muzzin et al. 2009). In addition, Marchesini et al. (2009) made a comprehensive study of the systematic and random uncertainties of the GSMF analysis. These authors used different sets of IMF, metallicity, SPS models and extinction curve in the SED modelling to quantify the systematic errors. It was found that the evidence for mass-dependent evolution, with the low-mass end evolving more rapidly than the high-mass end, is no longer robust when the systematic uncertainties from the set of SED-modelling assumptions are taken into account. This work follows a similar approach, but for the first time, it aims to understand how the assumed cosmological model affects the GSMF. Therefore, the other set of parameters remain unchanged.

In order to verify the implication of the cosmological model on galaxy stellar mass determinations, we need at least two different cosmologies whose parameters are able to reproduce current observational constrains, such as those from supernovae Ia (SNIa) and baryonic acoustic oscillation (BAO). For this purpose, besides the ΛCDM parametrization of the Friedmann–Lemaître–Robertson–Walker (FLRW) perfect fluid model, we chose the parametrization of García-Bellido & Haugbølle (2008) for the Lemaître–Tolman–Bondi (LTB) dust model. Moreover, an inhomogeneous cosmology such as LTB lies on many recent advances on the development of this model (e.g. Alfedeel & Hellaby 2010;

Hellaby 2012; Nishikawa, Yoo & Nakao 2012; Valkenburg, Marra & Clarkson 2012) and several tests and fits to different observables (e.g. February et al. 2010; Bolejko et al. 2011; Bull, Clifton & Ferreira 2012; Hoyle et al. 2013). Great effort has been made recently in order to establish inhomogeneous models as a viable alternative, or generalization, of the standard model.

From an observational perspective, recent papers sought for evidence of a large local void. Keenan, Barger & Cowie (2013) studied the K-band galaxy luminosity function (LF) from the UKIRT Infrared Deep Sky Large Area Survey (UKIDSS-LAS) and 2MASS Survey with spectroscopy from the Sloan Deep Sky Survey (SDSS), Two-degree Field Galaxy Redshift Survey (2dFGRS), Six-degree Field Galaxy Redshift Survey (6dFGRS) and Galaxy And Mass Assembly (GAMA), and found an underdense region inside a radius of about 300 h^{-1} Mpc at $z \leq 0.07$. Whitbourn & Shanks (2014) analysed the galaxy density distribution of $\sim$250 000 galaxies out to $z \sim 0.1$ based on the 2MASS K-band photometry and the combination of the 6dFRGS, GAMA and SDSS spectroscopic data for different sky regions: the South Galactic Cap (SGC), the southern part of the North Galactic Cap (NGC) and the northern part of the NGC. They found a large underdense region within a radius of 150 h^{-1} Mpc in the SGC, a less pronounced underdensity in the northern part of the NGC and no underdensity in the southern part of the NGC. If confirmed, an underdense region of 200–300 h^{-1} Mpc would explain the apparent tension between the direct measurements of the Hubble constant and those inferred by Planck, because any cosmology would have to account for the local void before fitting the SNIa Hubble diagram. However, Böhringer et al. (2015) argued differently. They studied the local density distribution in the southern sky with the ROSAT-ESO Flux-Limited X-ray galaxy cluster survey (REFLEX II) and compared results with the two papers mentioned previously. They found a local underdensity that is not isotropic and limited to a size significantly smaller than 300 Mpc radius. The authors stated that the other works that detect a local void are dominated by galaxy data preferentially from regions in the SGC near the equator and near the South Galactic Pole, which are indeed underdense, whereas other sky regions are not underdense at low redshift. Therefore, this topic still remains open to discussion.

It must be stressed that the approach of this work is very general, from the estimation of the stellar mass to the GSMF calculation. In addition, any other type of cosmology can be included in the calculation, like models based on modified gravity (e.g. Tsujikawa 2010) or the Szekeres solution (e.g. Peel, Ishak & Troxel 2012). The LTB model was chosen because it is a simple inhomogeneous model, but different enough from the standard Friedmann model so as to allow the comparison of the results.

In this work we start from the galaxy sample used by Ilbert et al. (2013), which was based on the data taken by the VIRCAM (Emerson & Sutherland 2010) on the VISTA telescope as a project named UltraVISTA. In order to reproduce the results of Ilbert et al. (2013) for a ΛCDM cosmology, we followed their approach to derive the GSMF, as well as the same sources and photometry. The galaxy sample was selected in the K_S band from the UltraVISTA data (McCracken et al. 2012) and the photometric redshifts were calculated using a 29-band multiwavelength catalogue that includes near-infrared filters from UltraVISTA, broad and intermediate/narrow bands from COSMOS (Capak et al. 2007), Infrared Array Camera (IRAC)-bands from *Spitzer* (Ilbert et al. 2010) and a near-ultraviolet (NUV) band from *GALEX* (Zamojski et al. 2007). Ilbert et al. (2013) estimated the GSMF up to $z = 4$ for a full, star-forming and quiescent sample in the standard cosmology. We aimed at using the same catalogue of Ilbert et al. (2013) to

perform our analysis in different cosmologies. We computed the stellar mass and the GSMF using the standard model, to guarantee a result with no systematics, as well as the void models described by Zumalacárregui et al. (2012). Finally, we compared the redshift evolution of the GSMF in the standard and the alternative models.

It is important to emphasize that this paper does not aim at selecting cosmological models. Although it uses alternative cosmologies and compare results with the standard model, our goal is to determine how robust is the stellar mass analysis under a change of a cosmological model constrained by observations. Moreover, this work focuses on the possible dependence between galaxy evolution and cosmology.

Other papers present similarities with this work due to the study of the effects of the cosmology in the observational analysis. Iribarrem et al. (2013) computed the far-infrared LF for the *Hershel*/PACS evolutionary probe survey assuming both the standard and void-LTB models. These authors concluded that the LF slopes at the faint-end depend on the cosmology, and therefore, either the standard model is overestimating the number density of faint sources or the void models are underestimating them. Marulli et al. (2012) described the effects of the cosmology dependence of the distance–redshift relation on the clustering of galaxies. Aside from the different goals and the different quantities under analysis, this work performs for the first time an SED-fitting adopting an alternative cosmological model.

The plan of the paper is as follows. Section 2 describes the general features of the multiwavelength catalogue and the galaxy classification applied to the data. In Section 3, we summarize the relevant theoretical concepts of the standard and void-LTB cosmological models. The methodology to estimate the stellar mass and the discussion of the results in the different cosmologies is presented in Section 4. In Section 5, we describe the procedure to obtain the GSMF. The results of the GSMF for the full, blue and red, galaxy sample in all cosmologies are presented and discussed in Section 6. Finally, in Section 7 we summarize our conclusions.

2 DATA DESCRIPTION

2.1 Multiwavelength

Our multiwavelength catalogue is fully described in Ilbert et al. (2013; hereafter I13). It uses observations on the four near-infrared filters, Y, J, H and K_S from the first UltraVISTA DR1 data release (McCracken et al. 2012) in the COSMOS field (2 deg^2) together with optical broad and intermediate-band data taken by Subaru on the COSMOS project (Capak et al. 2007). The optical bands are as follows: u^*, B_J, V_J, r^+, i^+, z^+, $IA427$, $IA464$, $IA484$, $IA505$, $IA527$, $IA574$, $IA624$, $IA679$, $IA709$, $IA738$, $IA767$, $IA827$, $NB711$, $NB816$. Moreover, it was added data on mid-infrared bands from *Spitzer* (Ilbert et al. 2010) and an NUV band from *GALEX* (Zamojski et al. 2007). From these data only sources at $K_S < 24$ with good image quality were selected, resulting in an effective area of 1.52 deg^2. Based on the catalogue, the photometric redshifts were derived by I13 using the Le Phare code (Arnouts et al. 1999; Ilbert et al. 2006). The accuracy of these results were tested against several spectroscopic samples, and it was found that at $i^+_{AB} < 22.5(z_{med} \sim 0.5)$ the precision is 1 per cent with less than 1 per cent of catastrophic failures, whereas at $z > 1.5$ the precision of the photo-z is 3 per cent for $i^+_{med} \sim 24$. The final data set consists of about 220 000 galaxies with $K_S < 24$ in the range $0.2 < z < 4.0$, and photometric information in 29 bands, which includes NUV, optical and IR regimes, and redshift.
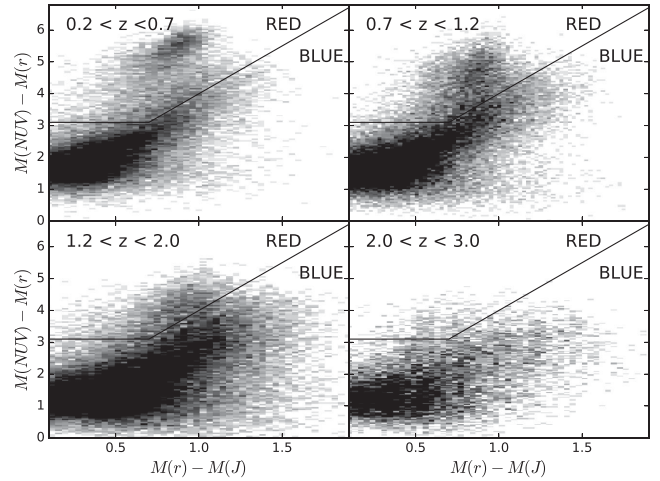

Figure 1. Two-colour classification of red and blue populations in the OCGBH model. The galaxies above the solid line in the top left are selected as quiescent (red) and those below the line are the star-forming ones (blue).

2.2 Galaxy classification

In addition to the total GSMF, we have also studied the effects of different cosmologies in the GSMF of blue and red galaxies separately. The sample was divided in 'red', also called 'quiescent', and 'blue', also referred as 'star-forming' galaxies. For this separation, following I13 we considered the rest-frame colour selection based on NUV$-r^+$ versus $r^+ - J$. The galaxies classified as quiescent have $M_{NUV} - M_r > 3(M_r - M_J) + 1$ and $M_{NUV} - M_r > 3.1$. This classification avoids a mix between dusty blue galaxies and red galaxies. Note that this criterion is applied to the analysis of both standard and void-LTB cosmologies. As an example, Fig. 1 shows the classification in the OCGBH model.

3 THEORETICAL FRAMEWORK

In this section, we will discuss the theoretical aspects of this work. We will present the differences of the cosmological concepts on both the LTB and ΛCDM models, as well as the divergences of the redshift evolution, the luminosity distance, time and comoving volume, in these two cosmologies.

3.1 LTB-void model versus standard model

The standard cosmological model fits very well the results from independent cosmological observables with a ΛCDM parametrization in the FLRW metric. This model assumes a perfect fluid energy–momentum tensor to solve Einstein's field equations using the FLRW line element, whose basic geometrical symmetries imply the spatial homogeneity and isotropy. A key result supporting the ΛCDM parametrization was the dimming in the redshift–distance relation of supernovae Ia (e.g.: Riess et al. 1998; Perlmutter et al. 1999), that is explained as an acceleration of the Universe's expansion rate. The current paradigm is that the acceleration is caused by an exotic fluid, namely dark energy, although we still do not know its physical nature.

The LTB model was successfully parametrized by García-Bellido & Haugbølle (2008) to fit simultaneously many independent observations without the cosmological constant. This model requires a pressure-less (dust) energy–momentum tensor in order to obtain an exact solution for the Einstein's field equations assuming an LTB

line element, and for this reason it is called as the LTB dust model. At early ages, when the radiation dominated the Universe's energy budget, the pressure term was relevant; however, at later ages the parametrization by Garcá-Bellido & Haugbølle (2008) makes the LTB solution to converge to a flat, spatially homogeneous universe. This last remark is important because it reconciles the model with the observed degree of isotropy found in the cosmic microwave background radiation maps. Therefore the non-homogeneity is a localized property of the model, that is, it has an effective under-dense region of Gpc scale around the Milky Way, rendering the name 'void models' to this parametrization. In this underdense region, the matter density profile Ω_M and the transverse Hubble constant H_0 are functions of the radial coordinate r. An interesting consequence from this model is that the extra dimming of distant supernovae Ia can be explained as an extra blueshift of the incoming light caused by a non-homogeneous distribution of matter in the line of sight.

3.2 Time, luminosity distance and comoving volume

There are two quantities involved in the estimation of the stellar mass which are affected by a change of cosmology: the luminosity distance and cosmic time. From the perspective of data analysis, a complete discussion on this topic is made in the next section. Here we aim at presenting the necessary theoretical equations to calculate these quantities and to show how they change with the chosen cosmology as function of the redshift. For the GSMF, we also have the comoving volume being affected due to the following relation:

$$\frac{dV_C}{dz} = r^2 \frac{dr}{dz}, \tag{1}$$

where both the radial coordinate $r(z)$ and its derivative dr/dz do change. Next, we will describe the key expressions to derive these quantities in both cosmologies.

The LTB line element ds_{LTB} in geometrized units ($c = G = 1$) can be written as below:

$$ds_{LTB}^2 = -dt^2 + \frac{A'(r,t)^2}{1 + \kappa(r)} dr^2 + A(r,t) d\Omega^2, \tag{2}$$

where $A'(r,t) = \partial A / \partial r$, $d\Omega$ is the spherical solid angle element, $A(r,t)$ the angular diameter distance and $\kappa(r)$ an arbitrary function. The following choice of the arbitrary functions, $A(r,t) = a(t)r$ and $\kappa(r) = kr^2$, reduces the previous expression to the FLRW line element $ds_{\Lambda CDM}$:

$$ds_{\Lambda CDM}^2 = -dt^2 + \frac{a(t)^2}{1 - kr^2} dr^2 + a(t)^2 r^2 d\Omega^2, \tag{3}$$

where $a(t)$ is the cosmic scalefactor and k is the curvature parameter ($k = +1, 0, -1$) in the FLRW metric.

We shall adopt a class of cosmological model with the LTB metric as given by equation (2) that characterize void models, that is, a pressureless content (dust) followed by an underdense matter profile $\Omega_M(r)$ around the Milky Way and a simultaneous big-bang time. This class is known as constrained García-Bellido & Haugbølle (2008), hereafter CGBH.

The CGBH model has five free parameters: the expansion rate H_{in} at the centre of the void, the underdensity value Ω_{in} at the centre of the void, the asymptotic density parameter Ω_{out} at large scales, the size R of the underdense region and the width ΔR of the transition between the central void and the exterior homogeneous region. We followed the parameter values proposed by Zumalacárregui et al. (2012) and also considered the case of an open universe

Table 1. Best-fitting values for the void-LTB models from Zumalacárregui et al. (2012) and the ones assumed for the ΛCDM models.

Parameter	CGBH	OCGBH
H_{in} (km s^{-1} Mpc^{-1})	66.0 ± 1.4	71.1 ± 2.8
Ω_{in}	0.22 ± 0.4	0.22 ± 0.4
R (Gpc)	$0.18^{+0.64}_{-0.18}$	$0.20^{+0.87}_{-0.19}$
ΔR (Gpc)	$2.56^{+0.28}_{-0.24}$	$1.33^{+0.36}_{-0.32}$
Ω_{out}	1	0.86 ± 0.33

Parameter	ΛCDM
H_0 (km s^{-1} Mpc^{-1})	70
$\Omega_{M,0}$	0.3
$\Omega_{\Lambda,0}$	0.7

($\Omega_{out} \leq 1$; hereafter OCGBH), which allows a better fit to the cosmic microwave background radiation.

For the void model, the matter density profile $\Omega_M(r)$ can be expressed as a function of the fit parameters as follows:

$$\Omega_M(r) = \Omega_{out} + (\Omega_{in} - \Omega_{out}) \left\{ \frac{1 - \tanh[(r - R)/2\Delta R]}{1 + \tanh[R/2\Delta R]} \right\}, \tag{4}$$

and the present-time transverse Hubble parameter $H_0(r)$ is given by:

$$H_0(r) = H_{in} \left[\frac{1}{\Omega_k(r)} - \frac{\Omega_M(r)}{\Omega_k(r)^{3/2}} \sin \, h^{-1} \sqrt{\frac{\Omega_k(r)}{\Omega_M(r)}} \right], \tag{5}$$

where $\Omega_k(r) = 1 - \Omega_M(r)$ is the curvature parameter inside the underdense region. Nevertheless, in the standard model both of these parameters show no dependence with the radial coordinate due to the spatial homogeneity assumption. Throughout this paper, we use the parameters presented in Table 1 for the LTB and ΛCDM models.

With these definitions, we can calculate the angular diameter distance $A(r, t)$ in a parametric form as below:

$$A(r, t) = \frac{\Omega_M(r)}{2[1 - \Omega_M]^{3/2}} [\cosh \eta - 1] A_0(r), \tag{6}$$

where A_0 is the angular distance at the present time, and the parameter η yields

$$\sinh \eta - \eta = 2 \frac{[1 - \Omega_M]^{3/2}}{\Omega_M} H_0 t. \tag{7}$$

Using the angular diameter $d_A = A[r(z), t(z)]$ we are able to calculate the luminosity distance d_L and the galaxy area distance d_G by means of the reciprocity theorem (Etherington 1933, 2007):

$$d_L = (1 + z)^2 d_A = (1 + z) d_G, \tag{8}$$

resulting in

$$d_L^{LTB} = (1 + z)^2 A[r(z), t(z)]. \tag{9}$$

For the FLRW metric, we also have the comoving-to-luminosity relation, $d_G = d_A(1 + z) = r$ as valid. Then using the expression

$$1 + z = \frac{a_0}{a(t)}, \tag{10}$$

one can reach the following expression:

$$d_A^{LCDM} = ra(t), \tag{11}$$

where the scalefactor at present time is $a_0 = 1$. Considering equation (8) we have that the luminosity distance in the ΛCDM model is given by

$$d_L^{\Lambda CDM} = (1 + z)^2 r(z) a[t(z)]. \tag{12}$$

The next step is to obtain $t(z)$ and $r(z)$ for both models. To do so we begin we must remember the radial null geodesic equation, $ds^2 = 0$, which, for equations (2) and (3), yield

$$\left.\frac{dt}{dr}\right|_{LTB} = -\frac{A'(r, t)}{\sqrt{1 - \kappa(r)}}. \tag{13}$$

$$\left.\frac{dt}{dr}\right|_{\Lambda CDM} = -\frac{a(t)}{\sqrt{1 - kr^2}}. \tag{14}$$

Assuming an LTB metric the relationship between time and redshift can be obtained from the redshift definition (e.g. Bondi 1947; see also Ribeiro 1992, pp. 5–6; Nogueira 2013, pp. 33–38):

$$\left.\frac{dt}{dz}\right|_{LTB} = -\frac{1}{1 + z}\frac{A'}{\dot{A}'}, \tag{15}$$

where $\dot{A}' = \partial A'/\partial t$, and the corresponding ΛCDM is given by,

$$\left.\frac{dt}{dz}\right|_{\Lambda CDM} = -\frac{1}{1 + z}\frac{a}{\dot{a}}, \tag{16}$$

where $\dot{a} = da/dt$. Combining equations (13) and (14) with equation (15) and (16) we are able to write below the radial coordinate r in terms of the redshift z for LTB metric,

$$\left.\frac{dr}{dz}\right|_{LTB} = \frac{1}{1 + z}\frac{\sqrt{1 - \kappa(r)}}{\dot{A}'}. \tag{17}$$

In order to reach at a model suitable for our purposes, the arbitrary function $\kappa(r)$ will be defined as follows:

$$\kappa(r) = -\Omega_k H_0^2(r)r^2. \tag{18}$$

For the ΛCDM model we have that

$$\left.\frac{dr}{dz}\right|_{LCDM} = \frac{1}{1 + z}\frac{\sqrt{1 - kr^2}}{\dot{a}}. \tag{19}$$

By solving equations (15) and (16), we can compare the behaviour of time in terms of the redshift in both cosmologies. Moreover, the solution of equations (17) and (19) advance the luminosity distance evolution in terms of the redshift as expressed in equations (9) and (12). Assuming for both models the free parameters presented in Table 1, we can compare the results of these quantities as function of the redshift in Fig. 2. The luminosity distance was then plotted as a logarithm of the ratio between the values in the different cosmologies to better compare with the stellar mass results.

It is interesting to note that the same metric, LTB, with different parameters, CGBH and OCGBH, renders a different luminosity distance evolution. This difference is such that in CGBH for $z < 1$ the luminosity distance exhibits values up to 6 per cent larger than ΛCDM, while in OCGBH the luminosity distance is up to 6 per cent lower than in ΛCDM. Another feature that can be seen in Fig. 2 is the rate at which the distinction between the values of d_L in the standard and void models evolves with redshift. Up to $z = 2$ this rate is prominent in both the CGBH and OCGBH models, but after this redshift value the rate of the difference becomes very stable, almost constant. In numbers, the discrepancies of $\log d_L$ with respect to the standard model for OCGBH range from 0.45 per cent at $z = 0.2$ to 14.60 per cent at $z = 4.0$, whereas for CGBH it varies from -5.51 per cent at $z = 0.2$ to 7.96 per cent at $z = 4.0$. The negative value for CGBH is related to $d_L^{CGBH} > d_L^{\Lambda CDM}$ up to $z \sim 1$.
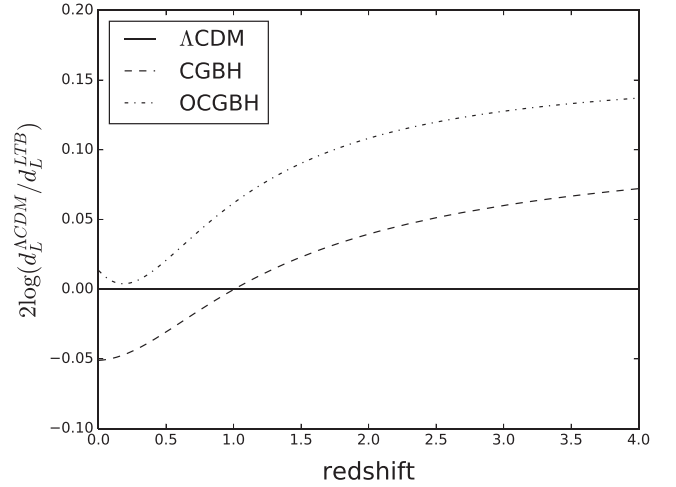

Figure 2. Ratio between the luminosity distance in the standard ΛCDM and the void-LTB models in terms of the redshift. By definition if this ratio is positive it means that $d_L^{\Lambda CDM} > d_L^{LTB}$, whereas a negative ratio means that $d_L^{\Lambda CDM} < d_L^{LTB}$. The LTB index stands for either CGBH or OCGBH and the solid line is for comparison results to be shown below.
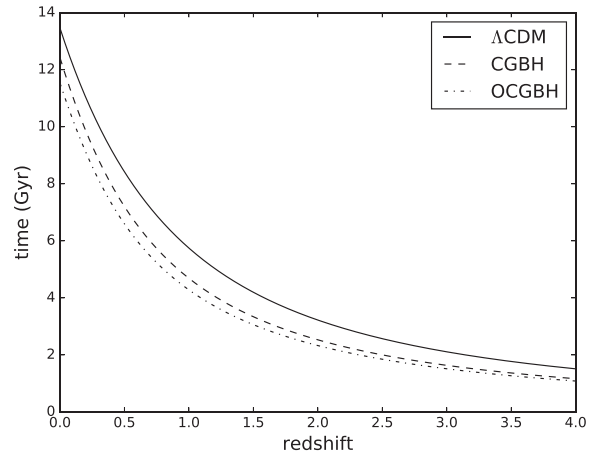

Figure 3. Redshift evolution of the cosmological time for the standard and void-LTB models. The age of the Universe evolves similarly in all cosmologies; however, the ages in LTB are systematically smaller than the ones in ΛCDM.

The cosmological time, that is, the age of the Universe, in both LTB parametrization and up to $z = 4$ is always smaller than the one in the ΛCDM model as illustrated in Fig. 3. At $z = 0$ the cosmological time for the CGBH model is $\sim$7.7 per cent smaller than in ΛCDM one, whereas in OCGBH it is $\sim$14 per cent smaller. This difference increases with the redshift up to $z \approx 1.5$, where the reduction in time for the CGBH model is $\sim$20 per cent, and $\sim$27 per cent for the OCGBH one. For $z > 1.5$ these discrepancies show a small increase in the variation such that at $z = 4$ they are $\sim$23 per cent for CGBH and $\sim$28 per cent for OCGBH.

Once equations (17) and (19) are solved we can compute the comoving volume element dV_C in all models. Its redshift evolution is shown in Fig. 4. Up to $z \approx 0.6$ the evolution of this volume in all models are similar; however, at $0.6 < z < 4$ the difference in these volumes regarding the ΛCDM model are always lower, from a few to $\sim$39 per cent for OCGBH, and up to $\sim$25 per cent for CGBH.

The general distinctions in these quantities introduced by the different models can be seen in Figs 2, 3 and 4. However, it must
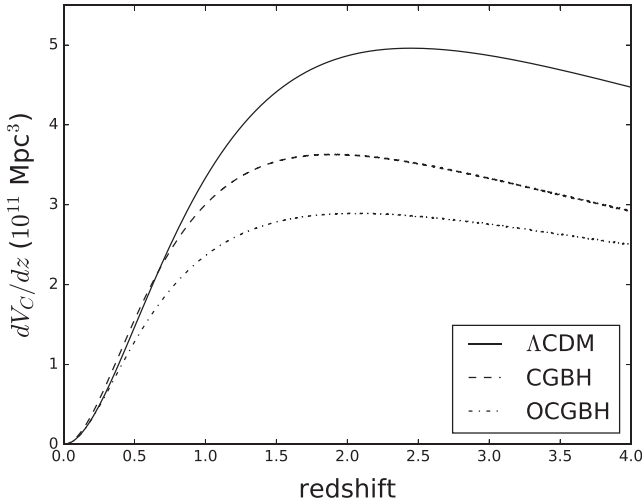
Figure 4. Comoving volume element for the standard (ΛCDM) and void models. This quantity evolves in a similar way in all models up to $z \approx 0.6$, then the ones based on the void models become smaller than ΛCDM.

be stressed that further variations might be added to the GSMF due to its calculation procedure based on the $1/V_{\mathrm{max}}$ method. This point will be better explained in Section 5.

4 STELLAR MASS ESTIMATION

The stellar mass was estimated using the public code *Photometric Analysis for Redshift Estimate*, or just *Le Phare* (Arnouts et al. 1999; Ilbert et al. 2006). Next, we shall describe how this code works to estimate the galaxy physical properties and what changes had to be made to allow the production of estimates in different cosmologies. Then, we will outline the input parameters used to derive the masses and present the results, as well as their respective discussions.

4.1 Le Phare

To convert the observational data from light to stellar mass we rely on the *Le Phare* package, which computes physical properties from galaxies applying a SED-fitting method. First, the procedure generates a synthetic spectral library based on a set of assumptions, such as the SPS models, filters, extinction law and *cosmology*. Then a template-fitting analysis is made between this library and a multi-wavelength catalogue. In other words, for each galaxy in the data set with a known redshift we fit the synthetic library to its photometric measurements. The result is a best-fitting SED for each source with the information about its physical properties.

As already mentioned, one of the priors to estimate the stellar mass is the cosmology. In the *Le Phare* package the established cosmology is the standard ΛCDM model and only the values of its parameters are allowed to change. However, if one wants to obtain the galaxy properties adopting an alternative cosmology, e.g. in non-homogeneous models or modified gravity, it is necessary to change the code.

For an analysis including only the luminosity, a change on the SED-fitting code would be unnecessary, and a simple relation among the luminosity in the standard model and the square of the ratio between the distances in both models is enough, as introduced by Iribarrem et al. (2013). However, we must consider an additional effect related to the stellar mass-to-light ratio $\mathcal{M}/L$. This quantity is a function of the SFH and, thus, it is related to time, which is a
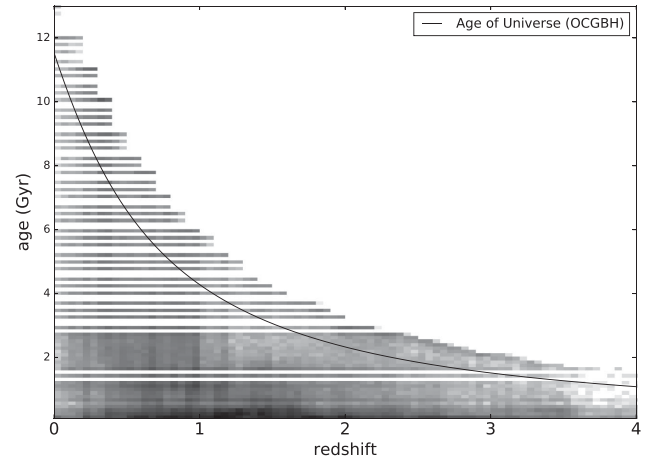

Figure 5. Age of the galaxies in the standard model versus redshift. This test was done using the ages derived by Ilbert et al. (2013). In this plot, the darker regions correspond to a higher number of galaxies. As it can be seen most of the galaxies are below the age of the Universe on the OCGBH model (solid line) and would not be affected by a change of the cosmological time. On the other hand, the ones above the solid line would not exist in the OCGBH model.

cosmology dependent quantity. Another way of understanding how the time affects the SED-fitting results is through the age of the galaxies. At a given z, the SED fitting puts a prior to the age of the galaxies being necessarily less than the age of the Universe. Nevertheless, as shown in Fig. 3, the age of the Universe in the LTB model, for both the CGBH and OCGBH parametrization, is always smaller than the one in the ΛCDM, resulting in galaxies, analysed by the latter model, with ages bigger than the age of the Universe in the alternative models. An example of this effect can be seen in Fig. 5 where the ages of the galaxies calculated using the 'unchanged' version of *Le Phare* are compared with the age of Universe in the OCGBH model. In order to guarantee the consistency of the output of the SED-fitting analysis, we also modified the function related to the cosmological time, replacing the standard model equations for time with commands that read a table with z and t and associate the t-values to the galaxy input z. Because of the prior on the age of the Universe, this modification causes a change in the number of available synthetic SEDs. We made modifications so that, instead of adopting the standard cosmology equations to compute the luminosity distance, it reads the values of a table containing z and d_{L}, then search for the luminosity distance d_{L} that corresponds to the galaxy z.

4.2 Stellar mass results

Once the modified version of *Le Phare* is ready, we can start to derive the stellar mass for the all cosmological models. We generated the library of synthetic spectra using the following set of assumptions: the SPS model of Bruzual & Charlot (2003); the Calzetti et al. (2000) extinction law; three metallicities ($Z = 0.004, 0.008, 0.02Z_{\odot}$, i.e. in units of solar metallicity); an SFH that falls exponentially, SFH $\propto \tau^{-1}\exp(-t/\tau)$, with nine possible values for τ from 0.1 to 30 Gyr; the extinction $E(B - V)$ ranges from 0 to 0.5, with an imposed prior of $E(B - V) < 0.15$ if age/$\tau > 4$ (Fontana et al. 2006; Pozzetti et al. 2007; Ilbert et al. 2010, 2013). These parameters remain the same for all cosmologies. We characterize the differences among the
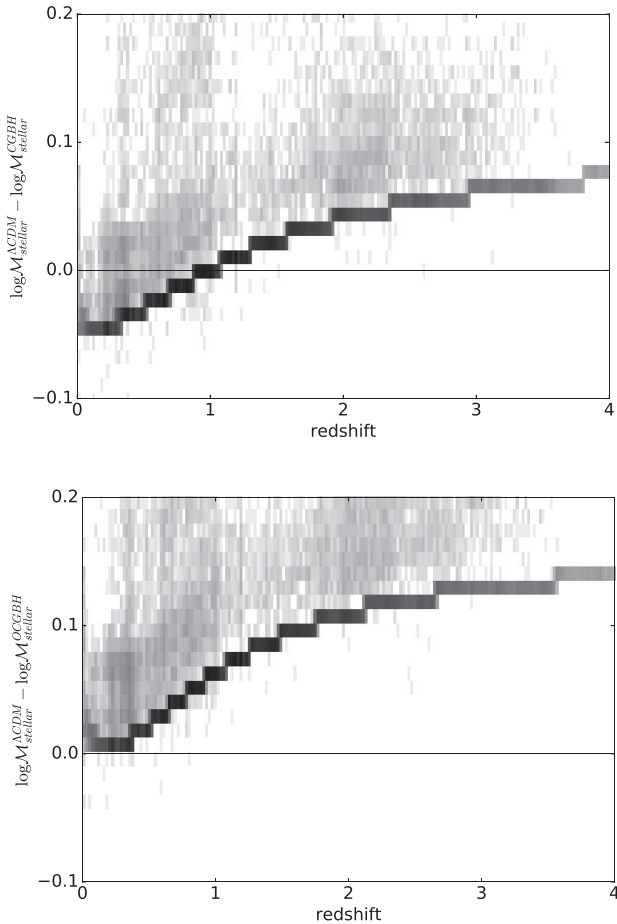
A. R. Lopes et al.

Figure 6. Average variation on the stellar masses from the CGBH model (*up panel*) and the OCGBH one (*down panel*) versus redshift. The solid line simplifies the correlation with Fig. 2. The darker region is where most of the galaxies are located. Note that this plot is a result of the output from *Le Phare*, so no completeness cut was applied.

stellar masses in different cosmological models through the simple relation

$$\Delta \log \mathcal{M}_{\text{stellar}} = \log \mathcal{M}_{\text{stellar}}^{\Lambda\text{CDM}} - \log \mathcal{M}_{\text{stellar}}^{\text{LTB}}, \qquad (20)$$

where the index LTB stands for CGBH or OCGBH, as shown in Fig. 6.

As expected the variation on the stellar mass for the LTB models compared to the ones for the standard model evolves with the redshift, which reflects the dependence on the luminosity distance and time with the redshift. A quick comparison between Figs 2 and 6 allows us to identify the contribution of the luminosity distance in the stellar mass result. The region where most of the galaxies are located can be directly linked to the effect caused by the change on the luminosity distance. Then, from a cosmological perspective, this distance bears the brunt of responsibility for the deviations on the stellar mass values. Moreover, we interpret the spread in the stellar mass difference as a consequence of the cosmological time variation. These conclusions seem to be consistent with the fact that most of the objects in the UltraVISTA sample are not be affected by a change of time-scale (Fig. 5). In the end, the masses of these galaxies reflect the combination of the effects due to two quantities, resulting in the spread observed in Fig. 6. In percentages, the reduction of the stellar mass due to the luminosity distance varies
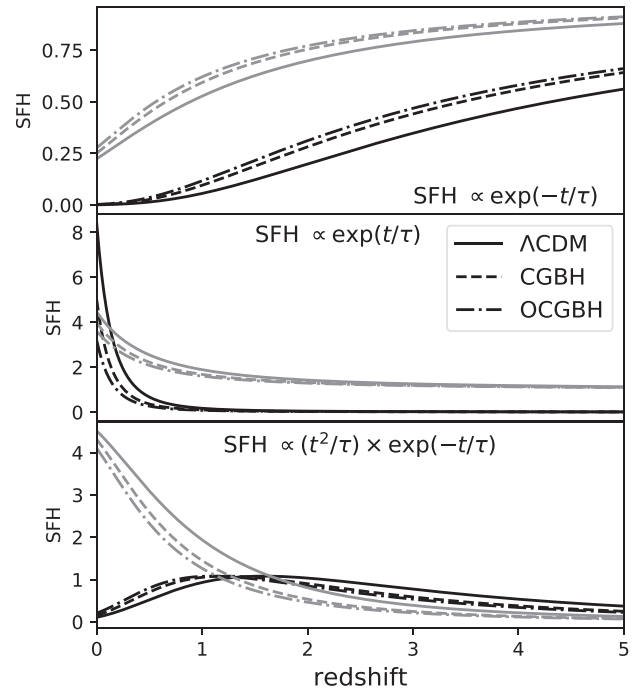

Figure 7. Three different parametrizations for the SFH in the standard and LTB models versus redshift. Each panel represents one of the following SFHs: exponentially decreasing law (*top panel*), inverted-τ law (*middle panel*) and delayed SFH (*bottom panel*). The black and grey lines respectively represent two values for τ, 2 and 9 Gyr. τ is the time-scale related to when the star formation began. The cosmological models are indicated by the line types: solid for ΛCDM, dashed for CGBH and dash–dotted for OCGBH.

from ~ 1.15 per cent to ~ 27.16 per cent for the OCGBH model, whereas for the CGBH model it varies from ~ -1.12 per cent to 15.20 per cent in the studied redshift range $0.2 < z < 4$. The negative values is related to $\mathcal{M}_{\text{stellar}}^{\text{CGBH}} > \mathcal{M}_{\text{stellar}}^{\Lambda\text{CDM}}$ at $z < 1$. However, for a smaller number of galaxies the time variation can render mass values up to about 40–50 per cent shorter in the LTB models than the ones in ΛCDM ones.

The variation due to the time-scale influences the SFH of galaxies. Fig. 7 shows three SFHs with two values for the star formation time-scale τ, 2 and 9 Gyr, assuming the LTB and standard models. This figure shows that changing the cosmological model leads to small changes in the SFH, less than one order of magnitude in all cases. However, depending on the SFH law galaxies can form more stars earlier in the LTB model than in the ΛCDM one (exponentially decreasing law; top panel), or more stars are formed earlier in the standard rather than the LTB models (inverted-τ law; middle panel). For the delayed SFH (bottom panel), the general behaviour depends on the value of τ. For $\tau = 2$ we have a mixed behaviour in which at $z < 1.5$ more stars are formed in the LTB cosmologies than in the ΛCDM model. At $z > 1.5$ the situation reverses, that is, for $\tau = 9$ the SFH behaves similarly to the inverted-τ law. Moreover, it is important to note that even in the cases where for a given SFH the general shape of the functions are not greatly affected by the different values of τ (top and middle panels), one can still see that for a given SFH law at a given z the difference among the results produced by the LTB and ΛCDM models show a dependence on the value of τ, i.e. on the top panel the SFH is similar for all cosmologies at $z < 0.5$ for $\tau = 2$, whereas for $\tau = 9$ the difference

MNRAS **471**, 3098–3111 (2017)

Downloaded from https://academic.oup.com/mnras/article/471/3/3098/3979469 by guest on 20 January 2021

of SFH is smaller for all models at $z > 3.5$. This effect may cause the SED-fitting code to choose different values of τ for different models, even assuming the same SFH. Or, even the same τ does not guarantee the same SFH at a given redshift.

For our analysis, in which only assumed an exponentially declining SFH, we verified that about 10 per cent of our galactic sample presents a change on the star formation time-scale τ, which means that stars begin to form at an earlier time in LTB than in ΛCDM. Nevertheless, to check if for a given cosmology a different SFH law is more efficient in describing the data, one should redo the whole analysis from the start assuming alternatives.

5 GALAXY STELLAR MASS FUNCTION

5.1 $1/V_{max}$ method

We chose to calculate the GSMF using the classical $1/V_{max}$ formalism (Schmidt 1968), which is a non-parametric estimator, i.e. it does not assume the shape of the GSMF. In a given redshift interval (z_1, z_2) each object i has a maximum redshift $z_{max, i}$ and a minimum redshift $z_{min, i}$ at which a source would still be included in the survey, assuming the $K < 24$ selection. In this work we considered the $z_{min, i}$ as the lower limit of redshift bin, therefore $z_{min, i} = z_1$. Then, the mass function for each mass bin centred in $\mathcal{M}_j$ is computed as follows:

$$\phi(\mathcal{M}_j)\,\Delta\mathcal{M}_j = \sum_i^N \frac{1}{V_{max,i}}, \tag{21}$$

where

$$V_{max} = \int_{z_1}^{\min(z_2, z_{max,i})} \Omega\, \frac{\mathrm{d}V(z)}{\mathrm{d}z}\mathrm{d}z, \tag{22}$$

N is the number of sources inside the mass bin and the redshift interval and Ω is the area covered by the survey.

To calculate z_{max} for each source with absolute magnitude M we have to solve the following equation:

$$M = 24 - 5\log d_L(z_{max}) - 25 - \mathrm{KC}(z_{max}), \tag{23}$$

where KC is the k-correction. From this expression it is clear that z_{max} is related to the luminosity distance, which depends on the cosmology. Consequently, z_{max} may change with the cosmological model.

An essential factor to account for when deriving the GSMF is the mass limit $\mathcal{M}_{lim}$, i.e. the minimum mass at which all galaxies would be observed at the given survey limit, $K_S \approx 24$. In other words, above this mass value the GSMF is considered to be complete. Following Pozzetti et al. (2010), for each source with mass $\mathcal{M}$ and apparent magnitude K we calculate the limiting mass as

$$\log(\mathcal{M}_{lim}) = \log(\mathcal{M}) + 0.4(K - 24). \tag{24}$$

The distribution of $\mathcal{M}_{lim}$ reflects the distribution of the mass-to-light ratio at each redshift. From this result we use the 20 per cent faintest galaxies at each redshift in order to avoid the influence of the brightest and reddest sources to compute the stellar mass completeness limit $\mathcal{M}_{com}$, defined as the mass value at which 90 per cent of the $\mathcal{M}_{lim}$ distribution lies below. It is important to note that this method differs slightly from the one adopted in Il13, where the authors based their estimates of $\mathcal{M}_{lim}$ on the 90 per cent most fitted

Table 2. Best-fitting parameters for double-Schechter function for the full galaxy sample adopting three different cosmologies.

| z-bin	$\log(\mathcal{M}_{com})$ $(\mathcal{M}_\odot)$	$\log(\mathcal{M}^*)$ $(\mathcal{M}_\odot)$	ϕ_1^* $(10^{-3}\,\mathrm{Mpc}^{-3})$	α_1	ϕ_2^* $(10^{-3}\,\mathrm{Mpc}^{-3})$	α_2
			ΛCDM model			
0.2–0.5	8.45	10.91 ± 0.07	1.55 ± 0.57	-1.08 ± 0.24	0.53 ± 0.35	-1.43 ± 0.08
0.5–0.8	8.88	11.00 ± 0.06	1.18 ± 0.38	-1.11 ± 0.20	0.13 ± 0.24	-1.63 ± 0.26
0.8–1.1	9.16	10.87 ± 0.08	1.87 ± 0.46	-0.76 ± 0.40	0.24 ± 0.48	-1.62 ± 0.33
1.1–1.5	9.42	10.68 ± 0.09	1.39 ± 0.36	-0.28 ± 0.45	0.60 ± 0.45	-1.47 ± 0.18
1.5–2.0	9.69	10.70 ± 0.11	0.86 ± 0.19	-0.36 ± 0.52	0.34 ± 0.14	-1.6
2.0–2.5	9.91	10.71 ± 0.08	0.63 ± 0.11	-0.23 ± 0.49	0.15 ± 0.08	-1.6
2.5–3.0	10.10	10.81 ± 0.09	0.18 ± 0.08	-0.15 ± 0.34	0.13 ± 0.03	-1.6
3.0–4.0	10.19	10.78 ± 0.45	0.02 ± 0.03	0.48 ± 1.05	0.08 ± 0.09	-1.6
			CGBH model			
0.2–0.5	8.47	10.85 ± 0.08	1.89 ± 0.66	-0.84 ± 0.25	0.63 ± 0.38	-1.42 ± 0.09
0.5–0.8	8.88	10.90 ± 0.07	1.64 ± 0.49	-0.90 ± 0.24	0.21 ± 0.24	-1.64 ± 0.20
0.8–1.1	9.15	10.86 ± 0.05	1.89 ± 0.35	-0.84 ± 0.15	0.25 ± 0.17	-1.61 ± 0.14
1.1–1.5	9.39	10.62 ± 0.10	1.67 ± 0.38	-0.43 ± 0.53	0.75 ± 0.37	-1.46 ± 0.21
1.5–2.0	9.65	10.62 ± 0.09	1.22 ± 0.22	-0.26 ± 0.47	0.49 ± 0.17	-1.6
2.0–2.5	9.84	10.65 ± 0.07	0.89 ± 0.15	-0.31 ± 0.47	0.19 ± 0.12	-1.6
2.5–3.0	10.02	10.72 ± 0.12	0.28 ± 0.13	-0.25 ± 0.89	0.18 ± 0.14	-1.6
3.0–4.0	10.10	10.68 ± 0.30	0.04 ± 0.03	0.40 ± 2.41	0.12 ± 0.11	-1.6
			OCGBH model			
0.2–0.5	8.42	10.77 ± 0.10	2.88 ± 0.50	-0.74 ± 0.18	0.78 ± 0.37	-1.44 ± 0.10
0.5–0.8	8.82	10.84 ± 0.07	2.04 ± 0.61	-0.90 ± 0.24	0.25 ± 0.31	-1.64 ± 0.20
0.8–1.1	9.08	10.77 ± 0.05	2.53 ± 0.45	-0.80 ± 0.16	0.34 ± 0.23	-1.61 ± 0.14
1.1–1.5	9.32	10.52 ± 0.07	2.26 ± 0.34	-0.34 ± 0.31	0.98 ± 0.21	-1.47 ± 0.27
1.5–2.0	9.58	10.54 ± 0.06	1.56 ± 0.17	-0.24 ± 0.28	0.64 ± 0.23	-1.6
2.0–2.5	9.77	10.55 ± 0.06	1.14 ± 0.18	-0.19 ± 0.43	0.27 ± 0.14	-1.6
2.5–3.0	9.94	10.60 ± 0.15	0.34 ± 0.13	-0.06 ± 0.82	0.28 ± 0.20	-1.6
3.0–4.0	10.03	10.63 ± 0.21	0.04 ± 0.02	0.37 ± 1.24	0.14 ± 0.09	-1.6
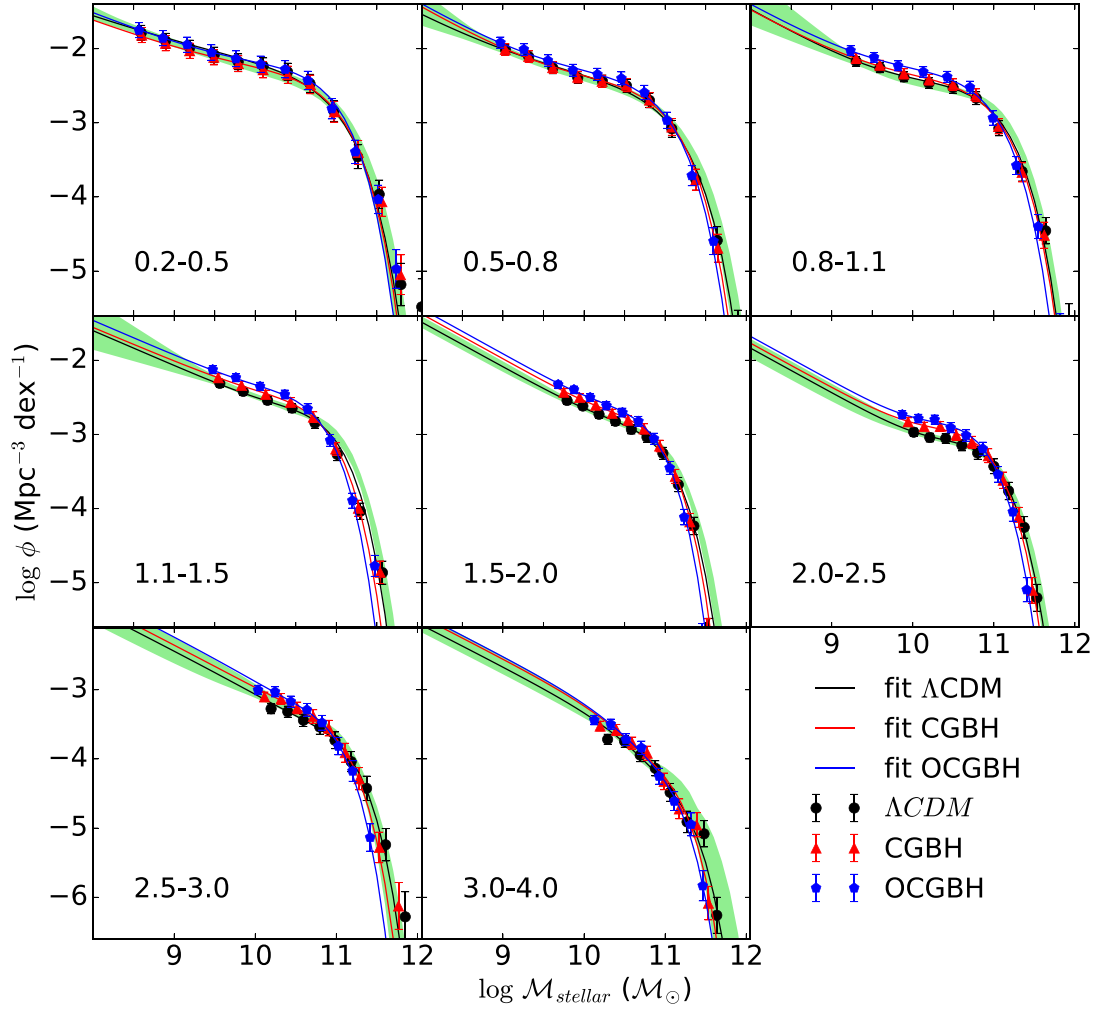
Figure 8. GSMF for the full galaxy sample in the standard (ΛCDM) and void-LTB (CGBH, OCGBH) models. Each panel corresponds to a specifically indicated redshift bin. The area represents the best fits from Ilbert et al. (2013) based on the same 220 000 *K*-select galaxies from UltraVISTA assuming the standard model. The lines are the best fits for each model and the symbols are as in the legend.

templates from the SED-fitting analysis instead of the 20 per cent faintest objects. This different procedure causes some discrepancies on the values of $\mathcal{M}_{com}$ from the standard model between this work and I13, mainly in the first bin $0.2 < z < 0.5$, where we find a more conservative values, about 0.52 dex higher. In the other bins the difference drops to <0.2 dex. We followed the same steps to obtain $\mathcal{M}_{com}$ in both ΛCDM and LTB models. The completeness mass in OCGBH becomes increasingly lower than in ΛCDM with the redshift, while for CGBH, the same pattern is seen but the values of $\mathcal{M}_{com}$ are closer to the ones in the standard model.

The total uncertainties associated to the GSMF are calculated using a combination of errors due to the template-fitting procedure σ_{fit}, the galaxy cosmic variance σ_{cosm_var} and Poissonian errors σ_{poiss}, given by

$$\sigma_{tot} = \sqrt{\sigma_{poiss}^2 + \sigma_{fit}^2 + \sigma_{cosm\_var}^2}, \tag{25}$$

where σ_{poiss} is derived from Poissonian statistics based on the $1/V_{max}$ method:

$$\sigma_{poiss}^2 = \left[\sum_i^N \frac{1}{V_{max,i}^2} \right]. \tag{26}$$

In order to obtain the cosmic variance in the standard model we use the public code `getcv` provided by Moster et al. (2011), which derives σ_{cosm_var} as

$$\sigma_{cosm\_var} = b\, \sigma_{DM}, \tag{27}$$

where b is the galaxy bias and σ_{DM} the dark matter variance related to the size of the observed field, 1.5 deg². The σ_{cosm_var} is computed as function of redshift and stellar mass bins, being, therefore, directly related to the GSMF data points. For the LTB models we assume that the cosmic variance is the same as in the standard model, which in practice is not valid. However, since the differences in the GSMF between different cosmologies are small, if the σ_{cosm_var} in LTB is bigger than the values we used, the significance of the difference in the GSMF would only be smaller, not causing a great impact in the conclusions we find in this paper. We will come back to this point in the next section.

For the σ_{fit} in the ΛCDM cosmology, we uses the results presented in I13. These values were based on a set of 30 mock catalogues which were created by perturbing each flux point according to its formal error measurements. Then, for each realization the stellar masses and the GSMF are recomputed and a 1σ dispersion of these results are obtained as function of mass and redshift. Based
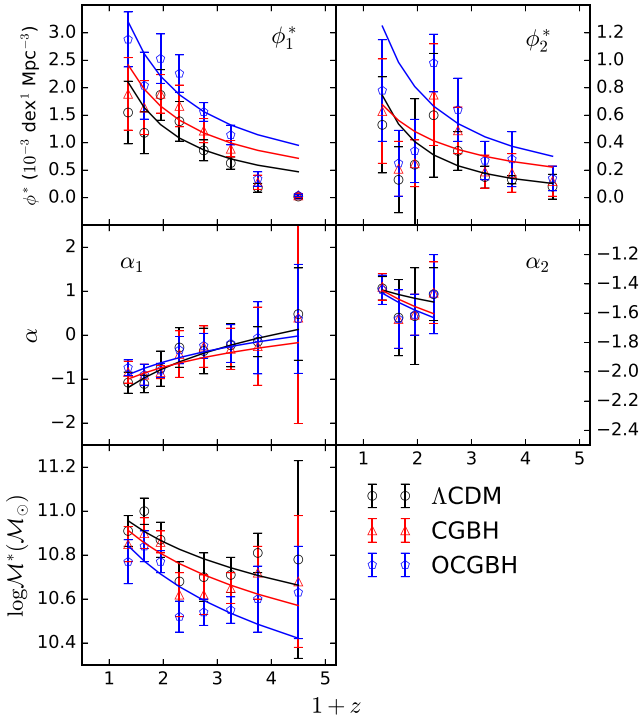
Figure 9. Redshift evolution of the five parameters of the double-Schechter function, $\phi*_1$, ϕ_2^*, α_1, α_2 and $\log \mathcal{M}^*$ of this work. Note that α_2 only has four points, because after $z = 2$ this parameter is no longer well-constrained and its value is fixed to -1.6.

on fig. 4 of Il13, it is straightforward to associate the curves in this plot to the GSMF data points. We chose to adopt the previously calculated σ_{fit} because we worked with the same galaxy data set and the same code to perform the SED-fitting. For the LTB models, we assumed that the relationship between σ_{fit}, mass and redshift remains the same as found in the ΛCDM model. As mentioned before the difference in mass is small, so there is no reason to expect a major change in σ_{fit}.

6 DISCUSSIONS

In order to obtain a parametric form based on the $1/V_{\max}$ results, we followed Pozzetti et al. (2010) and fitted the data points with a double Schechter form which may be written as below:

$$\phi(\mathcal{M}) \, d\mathcal{M} = e^{-\frac{\mathcal{M}}{\mathcal{M}^*}} \left[\phi_1^* \left(\frac{\mathcal{M}}{\mathcal{M}^*} \right)^{\alpha_1} + \phi_2^* \left(\frac{\mathcal{M}}{\mathcal{M}^*} \right)^{\alpha_2} \right] \frac{d\mathcal{M}}{\mathcal{M}^*}. \quad (28)$$

Here $\mathcal{M}^*$ is the characteristic mass, α_1 and α_2 are the slopes in which $\alpha_2 < \alpha_1$, and ϕ_1^* and ϕ_2^* are the GSMF normalization parameters. Following Il13, for the full sample and blue population, we arbitrarily adopted $\alpha = -1.6$ at $z > 1.5$ in all cosmologies since this parameter is no longer well constrained at this regime. This value is derived in the lower redshift bin where the data is enough to constrain it. For the red galaxies, we fitted a simple Schechter given by

$$\phi(\mathcal{M}) \, d\mathcal{M} = e^{-\frac{\mathcal{M}}{\mathcal{M}^*}} \left[\phi_1^* \left(\frac{\mathcal{M}}{\mathcal{M}^*} \right)^{\alpha_1} \right] \frac{d\mathcal{M}}{\mathcal{M}^*}, \quad (29)$$

to the data at $z > 0.5$, since we did not identify any upturn at low mass. We only used a double Schechter in the first bin, $0.2 < z < 0.5$.

Table 3. Double-Schechter evolution parameter in the ΛCDM and LTB models.

Parameter	Model	A	B
ϕ_1^*	ΛCDM	0.003 ± 0.002	-1.2 ± 0.3
	CGBH	0.003 ± 0.002	-1.0 ± 0.3
	OCGBH	0.004 ± 0.002	-1.0 ± 0.2
ϕ_2^*	ΛCDM	0.001 ± 0.002	-1.6 ± 0.7
	CGBH	0.0009 ± 0.0013	-0.9 ± 0.6
	OCGBH	0.002 ± 0.002	-1.1 ± 0.4
$\log(\mathcal{M}^*)$	ΛCDM	11.03 ± 0.08	-0.24 ± 0.07
	CGBH	11.00 ± 0.09	-0.28 ± 0.07
	OCGBH	10.95 ± 0.09	-0.35 ± 0.08
α_1	ΛCDM	1.1 ± 0.3	-1.5 ± 0.3
	CGBH	0.6 ± 0.3	-1.2 ± 0.4
	OCGBH	0.7 ± 0.2	-1.1 ± 0.3
α_2	ΛCDM	-1.4 ± 0.4	-0.2 ± 0.2
	CGBH	-1.4 ± 0.3	-0.3 ± 0.2
	OCGBH	-1.4 ± 0.4	-0.3 ± 0.2

6.1 Full sample

The best-fitting parameters for the full sample in the standard and LTB models are given in Table 2 along with the stellar mass completeness $\mathcal{M}_{\text{com}}$ for eight z-bins. Note that all best-fitting results described in this section were obtained using a procedure different from that considered by Il13, in which the authors also accounted for the Eddington bias. For this reason, our results in the ΛCDM model present a few discrepancies when compared with those of Il13.

We found that for the full sample in the three cosmological models the GSMF evolution is strongly mass-dependent, with the low-mass sources evolving more rapidly than the high-mass ones, as can be seen in Fig. 8. Therefore, the global conclusions obtained in the standard model remain valid in the void-LTB models. Moreover, it can be seen in this figure that the LTB models overestimate the number density of galaxies with $\log \mathcal{M} < 11$, and underestimate the number density of galaxies with $\log \mathcal{M} > 11$ if one compares with the ΛCDM results in the redshift range $0.5 < z < 4$.

According to the values described in Table 2, we can evaluate how significant are the differences between the best-fitting parameters from the double-Schechter function of the standard and LTB models using the ratio $\Delta X / \delta(\Delta X)$, where

$$\Delta X = X^{\Lambda\text{CDM}} - X^{\text{LTB}}, \quad (30)$$

$$\delta(\Delta X) = \sqrt{(\delta\alpha_{\Lambda\text{CDM}})^2 + (\delta\alpha_{\text{LTB}})^2}, \quad (31)$$

and X can be replaced by any of the double (or simple) Schechter parameters. We found that α_1, α_2 and ϕ_2^*, on average, do not exhibit a meaningful alteration on their values, whereas $\mathcal{M}^*$ and ϕ_1^* are more influenced by the introduction of different cosmologies. More specifically, we found that CGBH and OCGBH show a significance level $<1\sigma$ for all Schechter parameters, with the exception of ϕ_1^* where it goes up to 1.42σ for CGBH and 2.52σ for OCGBH, and $\mathcal{M}^*$ where it goes up to 1.73σ.

An interpretation for the differences found in the GSMF is given by the different redshift relationships of the luminosity distance and cosmological time in different cosmologies. That causes a non-negligible $\Delta \log \mathcal{M}_{\text{stellar}}$ resulting in different sources in each mass bin. Besides, the comoving volume together with the $z_{\max}$ values of
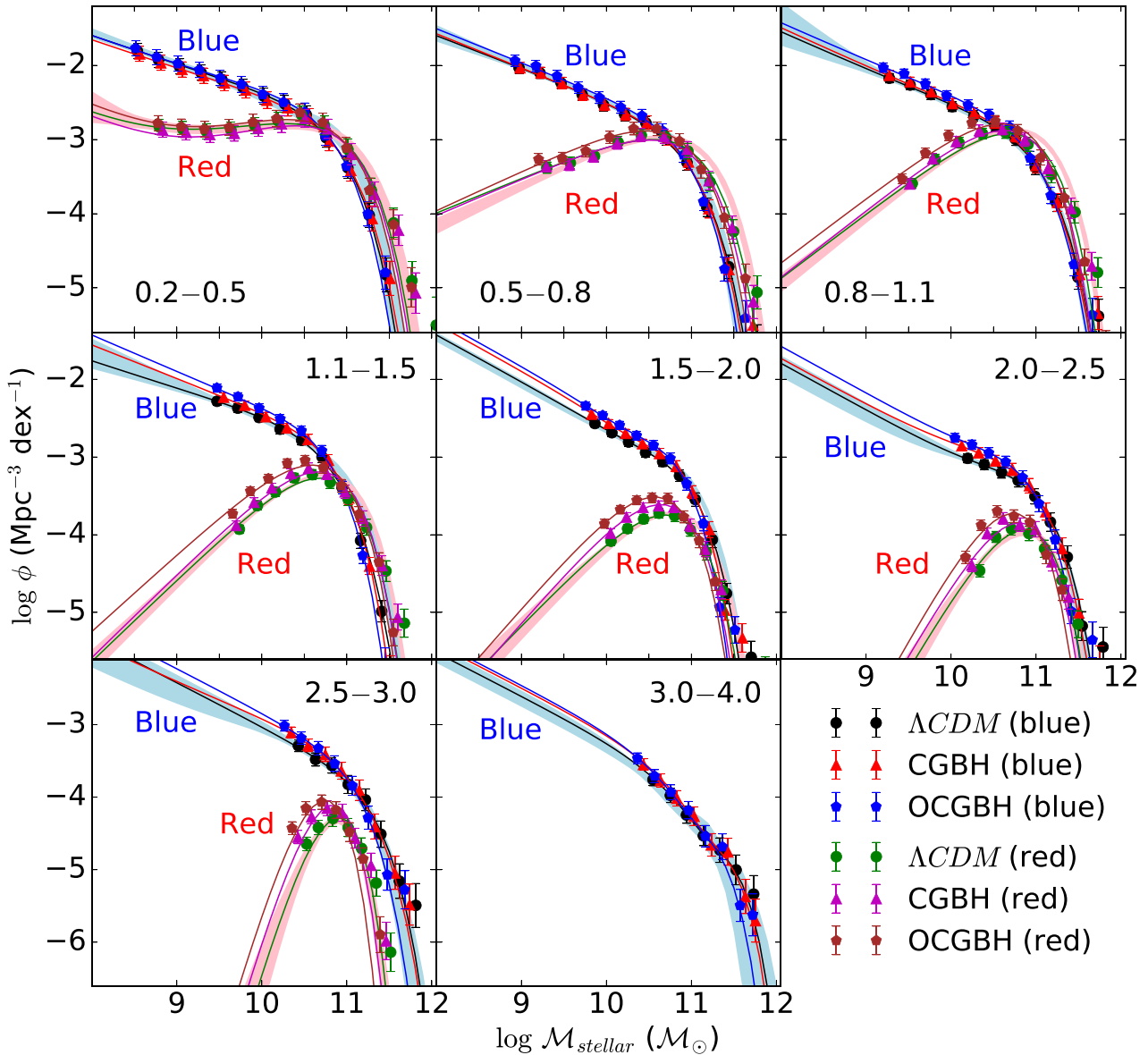
Figure 10. GSMF for the blue and red galaxy populations in the standard (ΛCDM) and void-LTB (CGBH, OCGBH) models. Each panel corresponds to a redshift bin. The blue and pink areas represent the best fits from Ilbert et al. (2013) for the blue and red galaxies, respectively. The solid lines are the best fits for each cosmological model. Symbols are as in the legend.

different cosmologies can lead to different values for $1/V_{max}$ even if the galaxies are the same in each mass bin.

Additionally, we investigated the redshift evolution of the double-Schechter parameters, as shown in Fig. 9. Let us assume that the parameters follow the expressions below:

$$\phi_1^*(z) = A_1(1+z)^{B_1}, \tag{32}$$

$$\phi_2^*(z) = A_2(1+z)^{B_2}, \tag{33}$$

$$\log[\mathcal{M}^*(z)] = A_3 + B_3 \ln(1+z), \tag{34}$$

$$\alpha_1(z) = A_4 + A_4 \ln(1+z), \tag{35}$$

$$\alpha_2(z) = A_5 + B_5 \ln(1+z), \tag{36}$$

where A_i and B_i are the evolution parameters and $i = 1, 2, 3, 4, 5$ with each number being related to one of the double-Schechter parameters. To fit the evolution functions described in equations (32)–(36) to their corresponding double-Schechter parameter results, we applied a least-squares technique. The uncertainties for each evolutionary parameter were obtained from the square root of the diagonal element of the covariance matrix. The best fits for the evolution parameters in each cosmology are listed in Table 3. There are no significant differences in the evolution of the parameters of the double-Schechter function in the void-LTB models as compared to the standard one.

Note that the GSMF depends on the definition of cosmological distances and time, However, these quantities depend non-linearly with the cosmology. Therefore, it is difficult to predict how a different cosmological model will affect the GSMF. Hence, for other cosmologies it is necessary to redo the whole calculation.

Table 4. Best-fitting parameters for double-Schechter function for the blue and red galaxy population adopting three different cosmologies.

z-bin	$\log(\mathcal{M}_{com})$ $(\mathcal{M}_\odot)$	$\log(\mathcal{M}^*)$ $(\mathcal{M}_\odot)$	ϕ_1^* $(10^{-3}\,\mathrm{Mpc}^{-3})$	α_1	ϕ_2^* $(10^{-3}\,\mathrm{Mpc}^{-3})$	α_2
			Blue galaxies			
			ΛCDM model			
0.2–0.5	8.40	10.73 ± 0.07	0.57 ± 0.33	-0.87 ± 0.40	0.87 ± 0.17	-1.40 ± 0.12
0.5–0.8	8.85	10.77 ± 0.24	0.29 ± 0.38	-0.50 ± 0.29	0.66 ± 0.30	-1.44 ± 0.05
0.8–1.1	9.15	10.83 ± 0.09	0.46 ± 0.33	-0.83 ± 0.58	0.44 ± 0.27	-1.51 ± 0.13
1.1–1.5	9.41	10.70 ± 0.08	0.40 ± 0.43	-0.93 ± 0.75	0.73 ± 0.38	-1.37 ± 0.13
1.5–2.0	9.77	10.66 ± 0.09	0.61 ± 0.13	-0.23 ± 0.55	0.40 ± 0.13	-1.6
2.0–2.5	10.10	10.78 ± 0.05	0.43 ± 0.08	-0.40 ± 0.24	0.16 ± 0.04	-1.6
2.5–3.0	10.34	10.96 ± 0.20	0.10 ± 0.08	-0.48 ± 1.28	0.11 ± 0.08	-1.6
3.0–4.0	10.40	10.89 ± 0.28	0.005 ± 0.003	1.76 ± 0.57	0.08 ± 0.01	-1.6
			CGBH model			
0.2–0.5	8.44	10.77 ± 0.15	0.53 ± 0.45	-0.90 ± 0.89	0.73 ± 0.47	-1.40 ± 0.12
0.5–0.8	8.86	10.72 ± 0.15	0.48 ± 0.36	-0.51 ± 0.26	0.65 ± 0.19	-1.46 ± 0.13
0.8–1.1	9.15	10.79 ± 0.13	0.59 ± 0.40	-0.81 ± 0.79	0.46 ± 0.39	-1.53 ± 0.44
1.1–1.5	9.43	10.56 ± 0.07	0.89 ± 0.48	-0.34 ± 0.57	0.96 ± 0.49	-1.43 ± 0.17
1.5–2.0	9.73	10.52 ± 0.05	0.87 ± 0.17	0.17 ± 0.43	0.69 ± 0.15	-1.6
2.0–2.5	10.03	10.75 ± 0.14	0.56 ± 0.18	-0.63 ± 0.93	0.18 ± 0.26	-1.6
2.5–3.0	10.25	11.00 ± 0.22	0.14 ± 0.36	-1.25 ± 1.78	0.08 ± 0.44	-1.6
3.0–4.0	10.34	10.84 ± 0.18	0.005 ± 0.006	1.81 ± 1.10	0.10 ± 0.05	-1.6
			OCGBH model			
0.2–0.5	8.39	10.64 ± 0.12	1.10 ± 0.55	-0.86 ± 0.23	0.88 ± 0.52	-1.41 ± 0.15
0.5–0.8	8.80	10.66 ± 0.13	0.63 ± 0.40	-0.51 ± 0.29	0.81 ± 0.23	-1.46 ± 0.14
0.8–1.1	9.08	10.75 ± 0.11	0.64 ± 0.54	-0.82 ± 0.93	0.64 ± 0.60	-1.51 ± 0.41
1.1–1.5	9.35	10.50 ± 0.09	1.22 ± 0.37	-0.46 ± 0.62	1.08 ± 0.38	-1.47 ± 0.18
1.5–2.0	9.66	10.44 ± 0.05	1.11 ± 0.21	0.18 ± 0.40	0.89 ± 0.18	-1.6
2.0–2.5	9.95	10.62 ± 0.10	0.73 ± 0.21	-0.36 ± 0.75	0.31 ± 0.25	-1.6
2.5–3.0	10.17	10.78 ± 0.34	0.19 ± 0.16	-0.51 ± 2.38	0.22 ± 0.32	-1.6
3.0–4.0	10.27	10.73 ± 0.15	0.01 ± 0.01	1.49 ± 1.18	0.14 ± 0.06	-1.6
			Red galaxies			
			ΛCDM model			
0.2–0.5	8.65	10.86 ± 0.05	1.31 ± 0.22	-0.69 ± 0.09	0.03 ± 0.02	-1.51 ± 0.18
0.5–0.8	9.15	10.87 ± 0.05	0.99 ± 0.16	-0.53 ± 0.08		
0.8–1.1	9.36	10.74 ± 0.05	1.41 ± 0.16	-0.13 ± 0.09		
1.1–1.5	9.56	10.66 ± 0.04	0.63 ± 0.05	0.05 ± 0.09		
1.5–2.0	9.94	10.64 ± 0.04	0.21 ± 0.01	0.13 ± 0.13		
2.0–2.5	10.09	10.59 ± 0.06	0.10 ± 0.01	0.90 ± 0.29		
2.5–3.0	10.29	10.29 ± 0.09	0.004 ± 0.005	3.14 ± 0.97		
			CGBH model			
0.2–0.5	8.69	10.81 ± 0.07	1.40 ± 0.32	-0.57 ± 0.10	0.03 ± 0.02	-1.51 ± 0.24
0.5–0.8	9.14	10.82 ± 0.04	0.99 ± 0.15	-0.51 ± 0.08		
0.8–1.1	9.35	10.68 ± 0.04	1.56 ± 0.17	-0.10 ± 0.09		
1.1–1.5	9.56	10.63 ± 0.03	0.76 ± 0.05	0.07 ± 0.08		
1.5–2.0	9.94	10.54 ± 0.03	0.28 ± 0.01	0.26 ± 0.13		
2.0–2.5	10.09	10.52 ± 0.05	0.12 ± 0.01	0.93 ± 0.21		
2.5–3.0	10.29	10.22 ± 0.12	0.006 ± 0.003	3.13 ± 0.92		
			OCGBH model			
0.2–0.5	8.63	10.77 ± 0.05	1.62 ± 0.27	-0.61 ± 0.10	0.04 ± 0.02	-1.53 ± 0.14
0.5–0.8	9.05	10.79 ± 0.04	1.21 ± 0.18	-0.52 ± 0.07		
0.8–1.1	9.26	10.65 ± 0.04	1.90 ± 0.20	-0.13 ± 0.08		
1.1–1.5	9.52	10.60 ± 0.03	0.93 ± 0.07	-0.009 ± 0.08		
1.5–2.0	9.87	10.47 ± 0.02	0.35 ± 0.02	0.26 ± 0.12		
2.0–2.5	10.02	10.43 ± 0.05	0.15 ± 0.02	1.01 ± 0.27		
2.5–3.0	10.21	10.13 ± 0.08	0.007 ± 0.007	3.13 ± 0.91		

6.2 Blue and red populations

The evolution of the GSMF for the blue and red galaxies in both the standard and void-LTB models is shown in Fig. 10. In agreement with Il13, we found that in the standard model the blue galaxies with low mass ($<10^{10.7 - 10.9}$) present a strong evolution, especially at $z > 2$, whereas the ones with high mass ($10^{11.6 - 11.8}$) show no evolution on density. However, for the red population the GSMF suggests a mass-dependent evolution at $z < 1$, whereas at $1 < z < 3$ a pure density evolution seems to be more reasonable, with most massive galaxies evolving at the same rate as the intermediate mass galaxies and the normalization parameter increasing continuously from $z = 3$ to $z = 1$. The interpretation is that the blue galaxies are forming new stellar populations; therefore, the massive blue galaxies are necessarily quenched, creating new red galaxies along the cosmic time. The differences between the GSMF in the standard and LTB models are small enough to allow the same physical interpretation in the LTB cosmology.

Moreover, we analysed the best-fitting parameters from the Schechter functions for the two populations in the standard and LTB models as listed in Table 4. Following the same approach introduced in the previous subsection, as discussed in equation (31), we found out that the significance level of the difference between the parameters derived in LTB with respect to ΛCDM for blue galaxies is less than 1σ for all the parameters at all z-bins, with an exception at $1.5 < z < 2.0$ for ϕ_2^* where it reaches $\sim 2\sigma$ in OCGBH, and at $1.1 < z < 2.5$ for ϕ_1^* and $\mathcal{M}^*$ where the significance goes up to $\sim 1.35\sigma$ and $\sim 2.13\sigma$ in CGBH and in OCGBH, respectively. As for the red galaxies, the significance of the difference for α_1 is always less than 1σ, for ϕ_1^* it reaches 5σ and 6σ for the CGBH and OCGBH models, respectively, while for $\mathcal{M}^*$ is $>1\sigma$ in all z-bins for the OCGBH model and $<1\sigma$ for CGBH one, except at $1.5 < z < 2.0$ where it becomes 2σ.

As noted for the full sample at $z > 0.5$ for both the red and blue populations, the LTB models overestimate the number of galaxies at $\mathcal{M} < 10^{11}\,\mathcal{M}_\odot$ and underestimate the number of galaxies with $\mathcal{M} > 10^{11}\,\mathcal{M}_\odot$ with respect to the standard model.

7 CONCLUSION

In this work, we studied how the cosmological model affects the stellar mass analysis. To do so, we used a sample of about 220 000 galaxies selected in the K_S band from the UltraVISTA catalogue in the redshift range $0.2 < z < 4$. We computed the stellar mass of this data set assuming the standard ΛCDM and the void-LTB models using a modified version of the open source code *Le Phare*, which allows the galactic physical properties to be estimated from an SED-fitting procedure in different cosmological models. These results enabled us to answer the first of two basic questions of this paper, which are the degree of dependence of the stellar mass estimation with the cosmological model and how strong this dependence is. From the cosmological perspective, we found out that the main source of discrepancy is the luminosity distance, which, on average, changes the masses up to ≈ 27 per cent at $z \sim 4$. A secondary quantity that affects the mass is the cosmological time, which although affecting a fewer number of galaxies, it can lead to objects with mass up to 40–50 per cent less massive.

Once the stellar masses are calculated, we proceeded to obtain the GSMF applying the $1/V_{\text{max}}$ methodology. The aim was to try to answer the question of how robust is the GSMF under a change of cosmology. This is in fact the main question of this paper. We found out that for the full sample of galaxies no meaningful difference in

α_1, α_2 and ϕ_2^* was seen in the studied redshift range, whereas $\mathcal{M}^*$ and ϕ_1^* suffer a slightly bigger influence on their values related to the introduction of different cosmologies, $<3\sigma$ significance. These differences are not strong enough to change the shape of the GSMF and, consequently, the physical interpretation of its behaviour.

Additionally, we analysed the red and blue populations and verified that the red galaxies seem to be more affected by the change of cosmology than the blue galaxies, particularly in number density of galaxies with an important variation, up to 5–6σ, on the values of ϕ^* for the red galaxies. However, these differences affect neither the shape nor the interpretation of the GSMF for these population.

We concluded that any LTB model well constrained by the combination of SNIa, CMB and BAO results are enough to yield a robust estimate for the GSMF. Moreover, all conclusions from the GSMF in the ΛCDM cosmology remain the same in the observationally constrained void-LTB models in the studied redshift range.

Although the technique discussed here can be applied to other cosmological models, the results obtained in this paper cannot be fully extended to other cosmologies because the cosmological dependence of the GSMF lies on the definition of the luminosity distance and cosmological time, which depend non-linearly with the cosmology. However, our results indicate that a consequence of the similarity between the redshift evolution of cosmological distance and time from two models, is that the GSMF will be robust under a change of cosmology between these models. Therefore, if a new model shows a redshift evolution for distance and time similar to the standard model, one should expect a similar GSMF in both models.

The next step in this line of investigation is to study the average galaxy mass from the UltraVISTA sample. We intend to use the GSMF results in this paper to proceed to the galaxy cosmological mass function analysis introduced by Lopes et al. (2014). This function consists of an alternative approach to the galaxy mass evolution, based in a combination of relativistic cosmology theory and observational quantities, such as GSMFs.

REFERENCES

Alfedeel A. H. A., Hellaby C., 2010, Gen. Rel. Grav., 42, 1935
Arnouts S., Cristiani S., Moscardini L., Matarrese S., Lucchin F., Fontana A., Giallongo E., 1999, MNRAS, 310, 540
Baldry I. K. et al., 2012, MNRAS, 421, 621
Böhringer H., Chon G., Bristow M., Collins C. A., 2015, A&A, 574, A26
Bolejko K., Hellaby C., Alfedeel A. H. A., 2011, J. Cosmology Astropart. Phys., 9, 11
Bondi H., 1947, MNRAS, 107, 410
Bruzual G., Charlot S., 2003, MNRAS, 344, 1000
Bull P., Clifton T., Ferreira P. G., 2012, Phys. Rev. D, 85, 024002
Calzetti D., Armus L., Bohlin R. C., Kinney A. L., Koornneef J., Storchi-Bergmann T., 2000, ApJ, 533, 682
Capak P. et al., 2007, ApJS, 172, 99
Cimatti A. et al., 2008, A&A, 482, 21
Conroy C., 2013, ARA&A, 51, 393
Conroy C., Gunn J. E., White M., 2009, ApJ, 699, 486
Domínguez-Sánchez H. et al., 2011, MNRAS, 417, 900
Emerson J. P., Sutherland W. J., 2010, in Stepp L. M., Gilmozzi R., Hall H. J., eds, Proc. SPIE Conf. Ser. Vol. 7733, Ground-based and Airborne Telescopes III. SPIE, Bellingham, p. 773306

Etherington I. M. H., 1933, Phil. Mag., 15, 761; reprinted in Gen. Rel. Grav. 39, 1055, 2007

February S., Larena J., Smith M., Clarkson C., 2010, MNRAS, 405, 2231

Fontana A. et al., 2006, A&A, 459, 745

García-Bellido J., Haugbølle T., 2008, J. Cosmology Astropart. Phys., 4, 3

Hellaby C., 2012, J. Cosmology Astropart. Phys., 1, 43

Hoyle B., Tojeiro R., Jimenez R., Heavens A., Clarkson C., Maartens R., 2013, ApJ, 762, L9

Ilbert O. et al., 2006, A&A, 457, 841

Ilbert O. et al., 2010, ApJ, 709, 644

Ilbert O. et al., 2013, A&A, 556, A55 (Il13)

Iribarrem A. et al., 2013, A&A, 558, A15

Joachimi B., 2016, in Skillen I., Barcells M., Trager S., eds, Proc. ASP Conf. Ser. Vol. 507, Multi-Object Spectroscopy in the Next Decade: Big Questions, Large Surveys, and Wide Fields. Astron. Soc. Pac., San Francisco, p. 401

Keenan R. C., Barger A. J., Cowie L. L., 2013, ApJ, 775, 62

Komatsu E. et al., 2009, ApJS, 180, 330

Lopes A. R., Iribarrem A., Ribeiro M. B., Stoeger W. R., 2014, A&A, 572, A27

Maraston C., 2005, MNRAS, 362, 799

Maraston C., Pforr J., Renzini A., Daddi E., Dickinson M., Cimatti A., Tonini C., 2010, MNRAS, 407, 830

Marchesini D., van Dokkum P. G., F''orster S., Natascha M., Franx M., Labbé I., Wuyts S., 2009, ApJ, 701, 1765

Marulli F., Bianchi D., Branchini E., Guzzo L., Moscardini L., Angulo R. E., 2012, MNRAS, 426, 2566

McCracken H. J. et al., 2012, A&A, 544, A156

McLure R. J., Cirasuolo M., Dunlop J. S., Foucaud S., Almaini O., 2009, MNRAS, 395, 2196

Mortlock A., Conselice C. J., Bluck A. F. L., Bauer A. E., Grützbauch R., Buitrago F., Ownsworth J., 2011, MNRAS, 413, 2845

Moster B. P., Somerville R. S., Newman J. A., Rix H., 2011, ApJ, 731, 113

Muzzin A., Marchesini D., van Dokkum P. G., Labbé I., Kriek M., Franx M., 2009, ApJ, 701, 1839

Nishikawa R., Yoo C.-M., Nakao K.-I., 2012, Phys. Rev. D, 85, 103511

Nogueira F. A. M. G., 2013, preprint (arXiv:1312.5005)

Peel A., Ishak M., Troxel M. A., 2012, Phys. Rev. D, 86, 123508

Perlmutter S. et al., 1999, ApJ, 517, 565

Pforr J., Maraston C., Tonini C., 2012, MNRAS, 422, 3285

Pozzetti L. et al., 2007, A&A, 474, 443

Pozzetti L. et al., 2010, A&A, 523, A13

Ribeiro M. B., 1992, ApJ, 388, 1

Riess A. G. et al., 1998, AJ, 116, 1009

Schmidt M., 1968, ApJ, 151, 393

Tsujikawa S., 2010, in Wolschin G., ed., Lecture Notes in Physics, Vol. 800, Cosmology Accelerated Expansion of the Universe. Springer-Verlag, Berlin, p. 99

Valkenburg W., Marra V., Clarkson C., 2012, MNRAS, 438, L6

Walcher J., Groves B., Budavári T., Dale D., 2011, Ap&SS, 331, 1

Whitbourn J. R., Shanks T., 2014, MNRAS, 437, 2146

Wuyts S. et al., 2007, ApJ, 655, 51

Zamojski M. A. et al., 2007, ApJS, 172, 468

Zumalacárregui M., García-Bellido J., Ruiz-Lapuente P., 2012, J. Cosmology Astropart. Phys., 10, 9

This paper has been typeset from a TEX/LATEX file prepared by the author.